HHS Public Access

Author manuscript

Glia. Author manuscript; available in PMC 2021 November 17.

Published in final edited form as:

Glia. 2021 September ; 69(9): 2199–2214. doi:10.1002/glia.24018.

Elevated fibroblast growth factor-inducible 14 expression transforms proneural-like gliomas into more aggressive and lethal brain cancer

Nina P. Connolly[1,2], **Rebeca Galisteo**[3,4], **Su Xu**[5,6], **Eli E. Bar**[1,2,7], **Sen Peng**[8], **Nhan L. Tran**[9], **Heather M. Ames**[2,7], **Anthony J. Kim**[1,2], **Graeme F. Woodworth**[1,2], **Jeffrey A. Winkles**[1,2,3,4]

[1]Department of Neurosurgery, University of Maryland School of Medicine, Baltimore, Maryland

[2]Marlene and Stewart Greenebaum Comprehensive Cancer Center, University of Maryland School of Medicine, Baltimore, Maryland

[3]Department of Surgery, University of Maryland School of Medicine, Baltimore, Maryland

[4]Center for Vascular and Inflammatory Diseases, University of Maryland School of Medicine, Baltimore, Maryland

[5]Department of Diagnostic Radiology and Nuclear Medicine, University of Maryland School of Medicine, Baltimore, Maryland

[6]Center for Advanced Imaging Research, University of Maryland School of Medicine, Baltimore, Maryland

[7]Department of Pathology, University of Maryland School of Medicine, Baltimore, Maryland

[8]Cancer and Cell Biology Division, Translational Genomics Research Institute, Phoenix, Arizona

[9]Departments of Cancer Biology and Neurosurgery, Mayo Clinic Arizona, Scottsdale, Arizona

Abstract

High-grade gliomas (HGGs) are aggressive, treatment-resistant, and often fatal human brain cancers. The TNF-like weak inducer of apoptosis (TWEAK)/fibroblast growth factor-inducible 14 (Fn14) signaling axis is involved in tissue repair after injury and constitutive signaling has

Correspondence Jeffrey A. Winkles, Department of Surgery, University of Maryland School of Medicine, 800 W. Baltimore St. Room 320, Baltimore, MD 21201. jwinkles@som.umaryland.edu.
Graeme F. Woodworth and Jeffrey A. Winkles are co-senior authors.

AUTHOR CONTRIBUTIONS

Nina P. Connolly, **Jeffrey A. Winkles**, and **Graeme F. Woodworth**: Conception and design. **Nina P. Connolly**, **Jeffrey A. Winkles**, and **Graeme F. Woodworth**: Development of methodology. **Nina P. Connolly**, **Rebeca Galisteo**, **Su Xu**, **Sen Peng**, and **Eli E. Bar**: Acquisition of data (provided animals, acquired and managed patients, provided facilities, etc.). **Nina P. Connolly**, **Su Xu**, **Sen Peng**, **Eli E. Bar**, **Nhan L. Tran**, **Heather M. Ames**, **Jeffrey A. Winkles**, and **Graeme F. Woodworth**: Analysis and interpretation of data (e.g., statistical analysis, biostatistics, computational analysis). **Nina P. Connolly**, **Rebeca Galisteo**, **Su Xu**, **Sen Peng**, **Eli E. Bar**, **Nhan L. Tran**, **Heather M. Ames**, **Anthony J. Kim**, **Jeffrey A. Winkles**, and **Graeme F. Woodworth**: Writing, review, and/or revision of the manuscript. **Nina P. Connolly**, **Rebeca Galisteo**, **Su Xu**, **Sen Peng**, and **Eli E. Bar**: Administrative, technical, or material support (i.e., reporting or organizing data, constructing databases). **Jeffrey A. Winkles** and **Graeme F. Woodworth**: Study supervision.

CONFLICT OF INTEREST

The authors declare no potential conflict of interest.

SUPPORTING INFORMATION

Additional supporting information may be found online in the Supporting information section at the end of this article.

been implicated in the pathogenesis of numerous solid cancers. The Fn14 gene is expressed at low levels in the normal, uninjured brain but is highly expressed in primary isocitrate dehydrogenase wild-type and recurrent HGGs. Fn14 signaling is implicated in numerous aspects of glioma biology including brain invasion and chemotherapy resistance, but whether Fn14 overexpression can directly promote tumor malignancy has not been reported. Here, we used the replication-competent avian sarcoma-leukosis virus/tumor virus A system to examine the impact of Fn14 expression on glioma development and pathobiology. We found that the sole addition of Fn14 to an established oncogenic cocktail previously shown to generate proneural-like gliomas led to the development of highly invasive and lethal brain cancer with striking biological features including extensive pseudopalisading necrosis, constitutive canonical and noncanonical NF-κB pathway signaling, and high plasminogen activator inhibitor-1 (PAI-1) expression. Analyses of HGG patient datasets revealed that high human PAI-1 gene (SERPINE1) expression correlates with shorter patient survival, and that the SERPINE1 and Fn14 (TNFRSF12A) genes are frequently co-expressed in bulk tumor tissues, in tumor subregions, and in malignant cells residing in the tumor microenvironment. These findings provide new insights into the potential importance of Fn14 in human HGG pathobiology and designate both the NF-κB signaling node and PAI-1 as potential targets for therapeutic intervention.

Keywords

Fn14; glioblastoma; high-grade glioma; NF-κB; PAI-1; RCAS/tv-a model

1 | INTRODUCTION

High-grade gliomas (HGGs) (WHO grade III and IV glial tumors) are aggressive brain tumors characterized by cellular and molecular heterogeneity, microvascular proliferation, immune system evasion, and brain invasion (Cloughesy et al., 2014; Khalafallah et al., 2020; Neftel et al., 2019; Quail & Joyce, 2017). These pathobiological characteristics, and the related treatment challenges unique to intrinsic brain tumors (Hersh et al., 2016; Woodworth et al., 2014), result in median survival in patients with glioblastoma (GBM, WHO grade IV gliomas) of less than 18 months (Stupp et al., 2017) with less than 10% surviving 5 years after diagnosis (Ostrom et al., 2020).

The TWEAK/Fn14 signaling axis is involved in tissue repair after injury and dysregulated signaling has been implicated in the pathogenesis of chronic inflammatory diseases and numerous solid cancers (Burkly et al., 2011; Winkles, 2008). In regard to HGGs, prior work has established that both TWEAK and Fn14 are expressed at low levels in normal brain and that Fn14, but not TWEAK, is highly expressed in (i) primary isocitrate dehydrogenase 1 (IDH1) wild-type and mesenchymal-subtype tumors; (ii) gliosarcoma, a particularly aggressive form of HGG; (iii) brain-invading tumor cells; and (iv) recurrent tumors (Fortin et al., 2009; Hersh, Harder, et al., 2018; Hersh, Peng, et al., 2018; Perez et al., 2016;Tran et al., 2003; Tran et al., 2006). Indeed, it has been reported that 70–85% of primary GBM tumors express high levels of Fn14 (Tran et al., 2003; Tran et al., 2006). Of note, Fn14 overexpression in glioma cells can activate NF-κB signaling in vitro (Tran et al., 2005) and an Fn14 mutant missing the extracellular, TWEAK binding domain can trigger this

same cellular response when expressed in an HEK293 NF-κB-luciferase reporter cell line (Brown et al., 2013). This suggests that TWEAK-independent Fn14 activation may be the primary mechanism of action in the pathobiology of GBM. In support of this possibility, several studies have shown that high Fn14 levels alone can promote glioma cell migration and invasion (Fortin et al., 2012; Roos et al., 2018; Tran et al., 2006) as well as resistance to chemotherapeutic drugs (Roos et al., 2017; Roos et al., 2018; Tran et al., 2005).

Our group has expanded the versatile replication-competent avian sarcoma-leukosis (RCAS)/tumor virus A (*tv-a*) modeling technology (Kanvinde et al., 2021) into the rat species to model in situ gliomagenesis, particularly tumor development and infiltration, over larger dimensions of time and space. In this prior work, we showed that intracranial delivery of RCAS constructs that produce platelet-derived growth factor-A (PDGF-A) overexpression and p53 depletion (via short hairpin [sh] RNA), an oncogenic cocktail previously shown to generate proneural-like gliomas in transgenic *nestin* or *GFAP* tv-a mice (Ozawa et al., 2014), had a similar biological effect in *nestin* tv-a rats (Connolly et al., 2017; Connolly et al., 2018). In the present study, we added an RCAS-Fn14 gene expression construct to the PDGF-A/shp53 cocktail to develop a model for human Fn14-overexpressing gliomas. We found that this single modification led to significantly shorter animal survival and transformed the proneural-like brain tumors into highly invasive, necrotic, and immune cell-rich gliomas. Two key molecular features of this Fn14-triggered transformation were (i) activation of canonical and noncanonical NF-κB signaling and (ii) increased expression of the multifunctional serine protease inhibitor (SERPIN) family member plasminogen activator inhibitor-1 (PAI-1). Finally, we uncovered a close correlation between human Fn14 (TNFRSF12A) and PAI-1 (SERPINE1) gene expression levels in distinct GBM tumor subregions and in individual tumor cells.

2 | MATERIALS AND METHODS

2.1 | Generation of rat brain tumors and animal survival analysis

All animal experiments were conducted in accordance with the University of Maryland School of Medicine (UMSOM) Institutional Care and Use Committee (IACUC) and followed NIH guidelines for animal welfare. The derivation of *nestin*/tv-a transgenic Sprague–Dawley rats, the construction of RCAS plasmids encoding either PDGF-A or p53 shRNA, transfection of these constructs into chicken DF-1 cells, and DF-1 cell injection procedure into neonatal brains have all been previously described (Connolly et al., 2017). The RCAS plasmid encoding Fn14, described by Fortin et al. (2012), was transfected into DF-1 cells and delivered via intracranial injection in the same manner. Rats were monitored daily until they developed brain tumor-related signs of illness (such as lethargy, weight loss, seizure, or paralysis) at which time they were euthanized. Rat survival curves were generated as described below comparing rats harboring Fn14-low (16 males, 15 females) or Fn14-high (12 males, 7 females) tumors.

2.2 | Gene expression and GBM patient survival analysis

Human survival datasets for Fn14, SERPINE1, and platelet-derived growth factor-B (PDGF-B gene (PDGFB)) were obtained through the GlioVis data portal to visualize and analyze

brain tumor gene expression (Bowman et al., 2017). In gene expression databases, the Fn14 gene is listed as TNFRSF12A, but the Fn14 nomenclature will be used in this report. The cut-off for low and high mRNA expression was determined based on the median value predetermined by the GlioVis portal software (Fn14 median: 7.43; SERPINE1 median: 8.38; PDGFB median: 8.93). All samples with mRNA expression above the median expression value were considered as “high” expressing and anything below the value was considered “low” expressing. Sample numbers and sexes: Fn14-low: 28 males, 20 females, 8 unspecified; Fn14-high: 109 males, 65 females, 10 unspecified; SERPINE1-low: 28 males, 19 females, 7 unspecified; SERPINE1-high: 106 males, 67 females, 12 unspecified; PDGF-B-low: 41 males, 37 females, 10 unspecified; PDGFB-high: 134 males, 86 females, 9 unspecified.

2.3 | Magnetic resonance imaging and spectroscopy

Magnetic resonance imaging (MRI) and MR spectroscopy (MRS) were used to monitor brain tumor growth as described previously (Connolly et al., 2017). All MRI scans were performed using a Bruker BioSpec 70/30USR Advance III 7T horizontal bore MR scanner (Bruker Biospin MRI) equipped with a BGA12S gradient system and interfaced to a Bruker Paravision 5.1 console. An MR compatible small-animal monitoring and gating system (SA Instruments Inc.) was used to monitor animal respiration rate and body temperature which was maintained at 37–38.5°C using a warm water bath circulation. LCModel package (version 6.3-0G; LCModel Inc.) (Provencher, 2001) was used for quantification of the MRS data. The reliability of the major biochemical entities was estimated in the Cramér–Rao lower bounds (CRLB) from the LCModel analysis. LCModel package was used for quantification of the MRS data. The primary biochemical entities' reliability was estimated in the CRLB from the LC Model analysis.

2.4 | Brain tissue collection

All brain tissue used for immunohistochemistry (IHC) and immunofluorescence (IF) was collected and processed as previously described (Connolly et al., 2017). Tissue collected for the protein profiling experiment included unfixed normal brain cortical tissue and tumor tissue (isolated from tumor-bearing brain cortex) which were flash-frozen on dry ice.

2.5 | Brain tumor histopathological and IHC analyses

Deidentified human GBM tissue specimens (formalin-fixed, paraffin-embedded) were obtained from the UMSOM Department of Pathology. Approval by the UMSOM Institutional Research Board was obtained before collecting the archived tissue. Tissues were processed by the University of Maryland Pathobiology Biorepository Share Services following the same protocol as previously reported (Hersh, Peng, et al., 2018). H&E staining and IHC analysis for Fn14 expression (1:200 dilution of Fn14 antibody ab109365, Abcam) and Ki-67 expression (1:100 dilution of Ki-67 antibody 275R-18, Sigma-Aldrich) was conducted by NDB Bio, LLC (Baltimore, MD) as follows. Fixed tissues were mounted in paraffin blocks using the Leica EG 1160 embedding center (Leica Microsystems) and then sectioned into 5 μm slices oriented in the coronal plane. For IHC, antigen retrieval was performed using either Bond Epitope Retrieval Solution1 (pH ~6) or Bond Epitope Retrieval Solution 2 (pH ~9) (Leica Microsystems) at 99–100°C for 20–32 min. IHC staining was

performed on a Leica BOND-III autostainer (Leica Microsystems) and peroxidase/DAB Bond Polymer Refine Detection System (Leica Microsystems) was used for Fn14 detection. For quantitation of the Ki-67 IHC results, three images were collected at ×20 magnification for each tumor type at distinct tumor locations. Positively labeled cells were counted using the Cell Count plugin on the Fiji ImageJ software (Schindelin et al., 2012). Each count was then divided by the image area (height in micrometers × width in micrometers converted into millimeters) to give the cells/area (mm^2).

2.6 | Brain tumor IF analysis

Coronal cryosections (12 μm) of rat brains were obtained from the center of the tumor's anterior–posterior extent. Tissues were blocked for 1 h in 2% donkey serum with 0.2% Triton X-100/0.02% Tween and labeled overnight at 4°C with the following primary antibodies: PAI-1 (1:1000; ab66705, Abcam), NF-κB p100/52 (1:100; NB100-82063, Novus Biological), CD163 (1:100; bs-2527R-TR, Bioss), CD68 (1:100; MAB 1435, Millipore), Iba1 (1:500; ab178846, Abcam), and CD49d (1:200; ab22858, Abcam). Alexa Fluor 488 (1:400, A-21202, Thermo Fisher Scientific) or Alexa Fluor 555 (1:400; A-31572, Thermo Fisher Scientific) secondary antibodies were applied, and tissues were coverslipped with ProLong Gold antifade reagent with DAPI (P36931; Thermo Fisher Scientific). Control tissue included normal brain tissue and omission of primary antibody on tumor tissue. Tissues were visualized using a W-1 spinning disk confocal microscope (Nikon Eclipse Ti-2). Quantitation of the IF results was performed as described for the IHC results.

2.7 | Western blot analysis and protein profiling using an antibody array

Normal brain tissue (cerebral cortex taken from an age-matched, normal Sprague–Dawley rat), Fn14-low and Fn14-high tumor tissue were lysed in HNTG buffer, disrupted using a tissue homogenizer, centrifuged to pellet debris, and the protein concentration in the supernatant determined using the BCA assay (Thermo Fisher Scientific). For Western blot analysis, equal amounts of protein were loaded into NU-PAGE SDS gels (Thermo Scientific) for electrophoresis followed by electrotransfer to PVDF membranes (Millipore). Membranes were blocked using 5% nonfat-milk in Tris-buffered saline with 0.1% Tween (TBST) (Cell Signaling Technology [CST]). Membranes were then incubated with either Fn14 (Abcam #109365), IκBα (CST #9242), RelB (CST #10544), NIK (CST #4994), p100/52 (CST #4882), or GAPDH (CST #2118) primary antibody and subsequently with an appropriate horseradish peroxidase (HRP)-conjugated secondary antibody (CST). The membranes were washed in TBST and HRP activity was determined by chemiluminescence using ECL Prime Western Blotting System (Millipore). Densitometric analysis of the Western blot data was performed using Fiji ImageJ software (Schindelin et al., 2012) and all tumor expression values were normalized to GAPDH levels and presented as fold expression relative to normal brain.

Protein profiling was performed using the Rat XL Cytokine Antibody Array Kit (R&D Systems ARY030) according to manufacturer's instructions. Equal amounts of protein (200 μg) in array buffer were added to nitrocellulose membranes containing 79 different capture antibodies printed in duplicate. Immunoreactive proteins were detected using

chemiluminescent reagents and densitometry was performed as described above to calculate relative signal intensities.

2.8 | Human normal (nonneoplastic) brain and GBM tumor gene expression analysis

PDGFB and SERPINE1 mRNA expression data corresponding to 10 normal brain and 548 GBM specimens were downloaded from the TCGA data portal (Level 3 data) (Cancer Genome Atlas Research Network, 2008) and analyzed as previously described (Hersh, Peng, et al., 2018).

2.9 | Human gene expression correlation analysis

TCGA_GBM low-grade gliomas (LGG) datasets were downloaded from the GlioVis data portal (Bowman et al., 2017) for the following genes: SERPINE1, TNFRSF12A (Fn14), and PDGFB. Each dataset includes GBM and LGG; however, only IDH wild-type patient samples were analyzed. Samples identified as “codel” were considered as IDH mutant with 1p/19q codeletion and were removed from the dataset and not included in the analysis (n = 496 samples total).

2.10 | Human gene expression analysis in distinct anatomic regions of GBM tumors

RNA-seq data from 122 morphologically distinct regions within 10 GBM tumors compiled through the Ivy Glioblastoma Atlas Project (Ivy GAP) (Puchalski et al., 2018) was used to analyze Fn14, SERPINE1, and RELB expression within morphologically distinct regions within GBM tumors. The data are presented as a heat map delineating the mRNA expression range in the tumor anatomic structures and in bar graphs showing relative expression values.

2.11 | Human GBM single-cell gene expression analysis

The expression level of Fn14 and SERPINE1 mRNAs in malignant and three nonmalignant GBM cell types (macrophages, oligodendrocytes, and T-cells) was determined by mining the single-cell RNA sequencing (scRNA-seq) dataset described by Neftel et al. (2019) and the results were displayed using violin plots as visualized using the Broad Institute single cell sequencing portal (https://singlecell.broadinstitute.org). The expression of Fn14 and SERPINE1 in single cells was extracted from the dataset and plotted to identify potential correlation.

2.12 | Statistical analyses

All analyses were conducted using GraphPad Prism statistical software, version 7.04. A p value of <.05 was considered significant for each analysis. Kaplan–Meier survival curves were generated and comparisons between the two gene expression level groups plotted on each curve were analyzed by the log-rank Mantel–Cox. Human GBM mRNA expression is presented as normalized z-scores, reflecting the number of standard deviations away from the mean of expression in the reference population, and evaluated using a two-tailed t test. Correlational data for both gene expression and single-cell data were analyzed to determine Pearson r correlations and p-values. RNA-seq data compiled by anatomic features from Ivy GAP was evaluated with Tukey's multiple comparisons test. The IHC and IF quantitation results were analyzed using a two-tailed t test.

3 | RESULTS

3.1 | Elevated Fn14 expression in both human and rat gliomas positively correlates with shorter survival

Kaplan–Meier survival curves comparing primary GBM patients with low or high Fn14 mRNA levels revealed that Fn14 overexpression correlates with a significant decrease in overall survival (Figure 1(a); 41.1 vs. 13.7 months, respectively; $p < .01$). We also found that human Fn14-low and Fn14-high tumor specimens exhibit some histopathological differences; for example, Fn14-high tumor core regions contained more areas with pseudopalisading features, and IHC analysis revealed that Fn14 levels were relatively high in these areas (Figure 1(b)).

We leveraged the RCAS/*tv-a* modeling system (Kanvinde et al., 2021), used previously by our group to study gliomagenesis in immunocompetent rats (Connolly et al., 2017; Connolly et al., 2018), to generate a model for Fn14-high human gliomas. One cohort of *tv-a* transgenic rat pups received an intracranial injection of equal amounts of DF-1 cells transfected with RCAS-PDGF-A and RCAS-shp53 constructs to serve as the Fn14-low group ($n = 31$) while another cohort received the same two constructs in equal combination with an RCAS-Fn14 construct to serve as the Fn14-high group ($n = 19$) (Figure 1(c)). These animals were observed over time and euthanized when they reached IACUC-designated criteria (e.g., weight loss, neurological symptoms). We found that the median survival for rats bearing Fn14-high tumors was shorter than that of the Fn14-low tumorbearing animals (Figure 1(d); 54 vs. 89 days, respectively, $p = .01$).

3.2 | Fn14-high rat gliomas demonstrated more tumor heterogeneity, altered metabolism, and a more infiltrative growth pattern compared to Fn14-low tumors

The two groups of experimental animals were monitored over time for tumor progression differences using MRI and MRS. Early in tumor development (14 days postinjection for Fn14-low and 30 days postinjection for Fn14-high), Fn14-low and Fn14-high tumors are visible mainly within the injected hemisphere (T_2-weighted image) without evidence of intratumoral blood products (T_1-weighted image) (Figure 2(a)). Importantly, at this earlier timepoint, Fn14-low tumors did not display increased vascular permeability, as evidenced by gadolinium-based contrast enhanced T_1-weighted imaging (T1C), whereas the Fn14-high tumors did show early T1C signal. As tumors progressed, the MRI differences became more striking: the Fn14-low tumors showing increasing intratumoral heterogeneity on T_1- and T_2-weighted imaging, and developing a significant T1C signal, but remaining relatively discrete from the surrounding brain with minimal evidence of vasogenic edema or tumor infiltration (Figure 2(a)). In contrast, the Fn14-high tumors developed a diffuse infiltrative pattern that often crossed the midline on T_2-weighted imaging and heterogeneous contrast-enhancement (T1C), consistent with new vascular permeability and disruption of the blood–brain barrier.

MRS data were also collected from both the tumor region and the contralateral cerebral hemisphere of Fn14-low and Fn14-high animals to compare cellular components and metabolic activity within these tissues, focusing on the clinically utilized metrics of choline to creatine (Cho:Cr) ratio, *N*-acetylaspartate (NAA) levels, and lactate levels. In comparison

to normal brain, both tumor types exhibited a progressive increase in the Cho:Cr ratio over time (Fn14-low early = 0.32 parts per million [ppm]; Fn14-low late = 0.94 ppm; 2.94-fold increase; Fn14-high early = 0.39 ppm; Fn14-high late = 0.64 ppm; 1.64-fold increase), consistent with increasing tumor proliferation (Figure 2(b)) (Chaumeil et al., 2015). There was a marked elevation in lactate levels later in the progression of Fn14-high tumors (early = 3.48 ppm; late = 11.22 ppm; 3.22-fold increase) compared to the corresponding Fn14-low tumors (early = 1.27 ppm; late = 1.77 ppm; 1.4-fold increase). Lactate accumulation in brain tumors is caused by increased anaerobic metabolism, and is associated with a more hypoxic and necrotic tumor microenvironment (TME; Chaumeil et al., 2015). Finally, NAA levels, generally considered an indicator of neuron density and health (Chaumeil et al., 2015), declined within Fn14-low tumors (early = 6.37 ppm; late = 0.66 ppm; 9.65-fold decrease) but remained relatively constant in Fn14-high tumors (early = 3.34 ppm; late = 3.20 ppm, 1.04-fold decrease) (Figure 2(b)). The difference in tumor NAA levels over the course of tumor growth and progression reflects an increasing displacement of neurons by the less invasive Fn14-low tumors, compared to persistent interspersion of neurons within the more invasive Fn14-high tumors. Together, these results demonstrate the significant in vivo differences between Fn14-high and Fn14-low tumors regarding both tumor metabolism and invasive growth patterns.

3.3 | Fn14-high rat gliomas overexpress Fn14, diffusely invade the brain, and have significantly more regions of pseudopalisading necrosis compared to Fn14-low tumors

Brains were collected from Fn14-low and Fn14-high tumor-bearing rats following euthanasia and processed for H&E staining as well as Fn14 and Ki-67 IHC analysis. As expected, Fn14-low tumors showed less Fn14 expression compared to Fn14-high tumors, which had widespread Fn14 expression in both tumor core cells and brain-invading glioma cells (Figure 3(a)).

Both tumor types demonstrated areas of microvascular proliferation, necrosis, and cellular atypia with numerous mitoses, consistent with high-grade (grade IV) gliomas. Close inspection of the H&E brain sections indicated that Fn14-low tumors were relatively smaller and had more well-defined edges, suggesting less invasion of tumor cells into surrounding brain tissues (Figure 3(b,c)). Conversely, in the Fn14-high tumors, infiltrating tumor cells diffusely invaded surrounding brain regions, particularly along white matter tracts and across the corpus callosum into the contralateral cerebral hemisphere. Perhaps, the most striking difference between the two tumor types was that the Fn14-high tumors exhibited more densely packed areas of pseudopalisading necrosis (Figure 3(b,d)) which is consistent with the high lactate level seen with MRS. While this feature could be found in some regions of the Fn14-low tumors, it is far more prevalent throughout the Fn14-high tumor core. Finally, we performed IHC analysis for Ki-67, a nuclear antigen specific to actively proliferating cells, to compare late timepoint tumor cell proliferative activity in Fn14-low and Fn14-high tumors. There was no significant difference in the normalized density (number of cells per unit area) of Ki-67-positive cells in the two tumor types (Supplemental Figure S1).

Tumor cell invasion and pseudopalisading necrosis were also prominent features of Fn14-high tumors even at the early stages of glioma development (Supplemental Figure

S2(a-c)). In addition, T_1-weighted contrast MRI demonstrated heterogeneous vascular permeability early in tumor development (Supplemental Figure S2(d)). T_2-weighted MRI of the same Fn14-high tumor revealed a less discrete, more infiltrative pattern consistent with tumor infiltration and vasogenic edema (Supplemental Figure S2(e), seen histologically in Supplemental Figure S2(c)).

3.4 | Fn14-high rat gliomas have more tumor-associated microglia/macrophages compared to Fn14-low tumors

The human GBM TME contains many noncancerous cell types, including both brain resident macrophages (microglia) and infiltrating bone marrow-derived macrophages, which together function as key mediators of malignancy and immune suppression (Gutmann & Kettenmann, 2019; Quail & Joyce, 2017). We reported previously that the rat Fn14-low, proneural-like glioma TME contains Iba1- and CD49d-positive cells (Connolly et al., 2017). In consideration of these findings, we compared tumor-associated macrophage (TAM) density in the Fn14-high rat gliomas and the Fn14-low gliomas by IF analysis using antibodies detecting four different TAM markers. This analysis revealed that another distinctive feature of the Fn14-high gliomas, compared to the Fn14-low gliomas, is increased TAMs in the TME (Figure 4(a)). Specifically, Fn14-high tumors showed a significantly higher density of cells expressing CD68 (activated M1-like macrophage), Iba1 (microglia/macrophage marker), CD163 (M2-like macrophage), and CD49d (bone marrow-derived macrophage marker) (Figure 4(b)).

3.5 | Elevated Fn14 expression in rat gliomas activates both the canonical and noncanonical NF-κB signaling pathways

Since TWEAK treatment of Fn14-positive glioma cells in vitro stimulates both the canonical (Roos et al., 2017; Tran et al., 2005; Tran et al., 2006) and noncanonical (Cherry et al., 2015) NF-κB pathways and Fn14 overexpression itself increases NF-κB signaling (Brown et al., 2013; Tran et al., 2005), we investigated NF-κB pathway status in normal brain, Fn14-low tumors, and Fn14-high tumors by Western blot analysis. We first confirmed elevated Fn14 expression in the Fn14-high tumor sample used for this analysis (Supplemental Figure S3 (a)) and then examined the expression level of three canonical NF-κB pathway-inducible proteins with negative feedback roles: IκBα (Sun et al., 1993), RelB (Bren et al., 2001), and p100 (NF-κB2) (Legarda-Addison & Ting, 2007). All of these proteins were expressed at higher levels in the Fn14-high tumors compared to normal brain and the Fn14-low tumors (Figure 5(a)). We confirmed the p100 Western blot data by IF analysis (Supplemental Figure S3(b,c)). In the p100 blot, we detected p100 proteolytic processing to p52, a crucial aspect of noncanonical NF-κB pathway activation (Tegowski & Baldwin, 2018). Therefore, to confirm that Fn14 overexpression in gliomas does activate the noncanonical NF-κB pathway, we examined the expression of the upstream serine/threonine kinase NIK, which accumulates in cells when this pathway is activated (Tegowski & Baldwin, 2018). NIK levels were also elevated in the Fn14-high tumors compared to both normal brain and the Fn14-low tumors (Figure 5(a)). These results demonstrate that Fn14 overexpression in rat gliomas activates the canonical and noncanonical NF-κB signaling nodes.

3.6 | Several secreted proteins, most notably, PDGF-B and PAI-1, are specifically expressed in Fn14-high rat gliomas

We screened for potential protein mediators of the aggressive Fn14-high tumor phenotype using normal brain, Fn14-low, and Fn14-high tissue lysates and an antibody array interrogating the expression level of 79 rat cytokines, chemokines, and growth factors. The expression level of many proteins, including the Fn14 ligand TWEAK, was similar in all three tissues but several proteins were expressed at higher levels in both tumor types compared to normal brain, most notably, lipocalin-2 and IGFBP-3 (Figure 5(b,c)). Of particular interest, there were four proteins expressed by Fn14-high tumors but not by Fn14-low tumors nor normal brain: PDGF-B (26.4-fold increase compared to normal brain), PAI-1 (22.9-fold), IGFBP-5 (8.8-fold), and osteopontin (OPN) (8.6-fold) (Figure 5(b,c); Table 1).

3.7 | The human PAI-1 gene (SERPINE1), but not the PDGF-B gene (PDGFB), is highly expressed in human GBM tumors, and its expression level correlates with shorter patient survival and the level of Fn14 expression

We interrogated several human glioma gene expression datasets to ascertain which of the top two Fn14-high tumor-specific proteins was more likely to play a role in Fn14-high human glioma pathobiology. First, we examined PDGFB and SERPINE1 mRNA expression levels in 10 normal brains and 548 GBM specimens using the TCGA data portal. We found that SERPINE1 mRNA levels, but not PDGFB mRNA levels, were significantly elevated in GBM specimens (Figure 6(a,b)). Second, Kaplan–Meier survival curves comparing primary GBM patients with low or high SERPINE1 or PDGFB mRNA expression were generated using the GlioVis data portal. We found that SERPINE1 overexpression, but not PDGFB overexpression, was an indicator of poor prognosis (SERPINE1-low: 43.9 months median survival, SERPINE1-high: 14.2 months; $p < .01$) (Figure 6(c,d)). Finally, we used the GlioVis data portal to determine whether there was a correlation between the Fn14 mRNA expression level and either the SERPINE1 or PDGFB mRNA expression level in IDH1 wild-type gliomas. This analysis revealed a more positive relationship between Fn14 and SERPINE1 gene expression, as evidenced by the more pronounced upward slope on the scatterplot and a higher Pearson correlation coefficient (r-value) (Figure 6(e,f)). Together, these findings, and IF data confirming increased PAI-1 protein levels in both rat and human Fn14-high tumors compared to the corresponding Fn14-low tumors (Supplemental Figure S4), informed us to further explore human Fn14 and SERPINE1 gene expression patterns in GBM tissues.

3.8 | The human Fn14, SERPINE1, and RELB genes are co-expressed in the same histological subregions of GBM tumors

In consideration of the positive correlation between Fn14 and SERPINE1 gene expression levels in bulk, heterogeneous glioma tissues, we evaluated the expression of these two genes in distinct anatomic regions of GBM tumors using the Ivy Gap database, which contains RNA-seq data from a collection of histologically defined, laser-microdissected areas of GBM tumors (Puchalski et al., 2018). We also included the RELB gene in this analysis since (i) it is highly expressed in rat Fn14-high tumors (Figure 5(a)) and in human mesenchymal-

subtype GBM (Verhaak et al., 2010; Zeng et al., 2019), (ii) its expression level correlates with shorter survival in GBM patients (Lee et al., 2013; Zeng et al., 2019), and (iii) the RelB protein has been reported to play a role in GBM tumorigenesis and inflammation (Lee et al., 2013; Waters et al., 2019). We found that the Fn14, SERPINE1, and RELB genes were expressed in all GBM regions, albeit to differing degrees. However, all three genes were most highly expressed in the same four regions: the perinecrotic zone, pseudopalisading cells around necrosis, hyperplastic blood vessels, and microvascular proliferation (Figure 7, Supplemental Figure S5).

3.9 | The human Fn14 and SERPINE1 genes are expressed by both tumor cells and tumor-associated macrophages residing in the GBM TME

One of the most notable properties of GBM tumors is their extensive cellular and molecular heterogeneity, and single-cell RNA sequencing (scRNA-seq) has emerged as a key platform to interrogate transcriptional profiles in malignant and tumor-supporting cell types (Khalafallah et al., 2020; Neftel et al., 2019). To gain insight into the cellular sources of Fn14 and PAI-1 protein expression in gliomas, we mined one of the GBM scRNA-seq databases for Fn14 and SERPINE1 gene expression and found that these genes were expressed by malignant cells and macrophages but not oligodendrocytes or T-cells within the TME (Figure 8(a)). In individual malignant cells, there was a statistically significant positive correlation between the Fn14 and SERPINE1 gene expression level (Figure 8(b)). A similar trend was observed in macrophages, but there were fewer pairs of data points (53 vs. 507 in malignant cells) and statistical significance was not reached.

4 | DISCUSSION

In this study, we examined the impact of high Fn14 levels on glioma biology using the RCAS/*tv-a*-based rodent model system and then dissected and validated these findings in human GBM tumor tissues and datasets. This work demonstrated that the sole addition of Fn14 to the proneural-like tumor-forming cocktail (PDGF-A/shp53) (Connolly et al., 2017; Connolly et al., 2018; Ozawa et al., 2014) generates more highly invasive and lethal tumors. The Fn14-high rat tumors displayed distinct pathological and molecular features not found in Fn14-low tumors, including (i) diffuse brain invasion with correspondingly elevated NAA levels, (ii) extensive pseudopalisading necrosis with associated high lactate levels, (iii) increased microglia/macrophage density, (iv) constitutive NF-κB pathway activation, and (v) elevated expression of several proteins, most notably, PDGF-B and PAI-1. Our analysis of human glioma datasets and the current literature supports the proposal that PAI-1 in particular could play an important role in the Fn14-high tumor phenotype.

The RCAS/*tv-a* system has proven to be a valuable tool to recapitulate key elements of human gliomas in an immunologically intact host microenvironment (Kanvinde et al., 2021). In our prior reports using this system, we showed that (i) elevated Fn14 expression in mouse astrocytes increased their proliferative and migratory capacity (Fortin et al., 2012), and (ii) combined PDGF-A overexpression and p53 depletion in rat neural precursor cells reproducibly generated brain tumors with many of the key features characteristic of mouse and human proneural-like gliomas (Connolly et al., 2017; Connolly et al., 2018). These

rat tumors express relatively low levels of Fn14 (Figures 3(a) and S3(a)); therefore, we delivered an Fn14 RCAS construct along with the PDGF-A and p53 shRNA constructs to develop a model for human Fn14-high gliomas. We found that the median survival for rats bearing Fn14-high tumors was significantly shorter than that of the Fn14-low tumor-bearing animals (54 vs. 89 days, respectively, $p = .01$). The updated median survival time reported here for rats harboring Fn14-low tumors aligns with the 92-day value found in our previous study (Connolly et al., 2017).

We compared Fn14-high and Fn14-low brain tumor progression by conducting MRI and MRS on live tumor-bearing rats and by histological and IF analyses of postmortem tumor tissues. The MRI and histological data indicated that the Fn14-high rat gliomas were more aggressive, heterogeneous, and invasive than their Fn14-low counterparts, consistent with the shorter survival time for Fn14-high tumor-bearing rats. Proton MRS was used to compare the Cho:Cr ratio, NAA levels, and lactate levels in normal brain and the two tumor types. We found that the Cho:Cr ratio was higher in both tumor types compared to normal brain. In human gliomas, a high Cho:Cr ratio is associated with higher cell proliferation, tumor grade, and worse patient prognosis (Chaumeil et al., 2015; Gao et al., 2019). NAA is produced by neurons and is considered a marker for neuronal density and overall health. Levels of this neuronal marker decreased during progression of the rat glial tumors, as is observed in human gliomas (Chaumeil et al., 2015; Kampa et al., 2020). The relatively higher NAA level in Fn14-high tumors (i.e., more neurons within the tumors) is consistent with the invasive growth pattern observed on MRI and in the histopathological analysis. The most prominent metabolic change noted in the Fn14-high tumors compared to both normal brain and the Fn14-low tumors was an elevation in lactate levels. Lactate is produced in cells that have shifted from aerobic to anaerobic glycolysis, which generally occurs in the setting of low oxygen levels (i.e., hypoxia). Hypoxia develops when tumors lose or outgrow their blood supply, which can happen due to a variety of factors, and it is a defining feature of high-grade brain tumors (Chaumeil et al., 2015; Kampa et al., 2020; Yang et al., 2012). This biochemical change in the Fn14-high tumors, in combination with the histological results showing vast regions of pseudopalisading necrosis, pathognomonic of HGG (Rong et al., 2006), is consistent with the idea that these tumors are more aggressive, hypoxic and necrotic than their Fn14-low counterparts. Another defining feature of the Fn14-high rat gliomas compared to the Fn14-low gliomas is an increase in both activated brain-resident microglia and infiltrating bone marrow-derived macrophages within the TME. These cells, collectively referred to as TAMs, can constitute up to ~30% of cells within human GBM tumors and have been shown to influence both glioma growth and responses to therapy (Gutmann & Kettenmann, 2019; Quail & Joyce, 2017).

The NF-κB signaling pathway is often constitutively activated in human gliomas and contributes to tumor pathobiology and therapeutic responses (Cahill et al., 2016; Friedmann-Morvinski et al., 2016). We have shown that Fn14 itself is an NF-κB target gene (Cheng et al., 2015; Tran et al., 2006); thus, this could explain, at least in part, why Fn14 is frequently overexpressed in human gliomas. Also, Fn14 signaling in glioma cells, initiated by either TWEAK engagement or Fn14 overexpression, can promote NF-κB activation (Cherry et al., 2015; Roos et al., 2017; Tran et al., 2005; Tran et al., 2006); therefore, Fn14 levels in tumors may be regulated by a positive feedback loop. Here, we show that Fn14-high gliomas exhibit

constitutive activation of the NF-κB signaling node. Of particular interest, we detected Fn14-triggered upregulation of two noncanonical NF-κB family members (RelB, p100), p100 processing to p52, and NIK accumulation, the latter two processes being hallmarks of noncanonical pathway activation (Tegowski & Baldwin, 2018). The noncanonical NF-κB pathway has generated increasing attention in the cancer biology field related to its pro-tumor functions, including roles in responding to chromosomal instability and co-opting chronic activation of innate immune pathways (Bakhoum et al., 2018; Tegowski & Baldwin, 2018). In gliomas, RelB function has been implicated in tumor growth, invasion, and stem cell maintenance (Cherry et al., 2015; Lee et al., 2013; Ohtsu et al., 2016). It has also been reported that NIK overexpression in glioma cells can increase tumor growth in an orthotopic mouse xenograft model (Cherry et al., 2015).

We used an antibody-based protein microarray to interrogate the expression level of rat cytokines, chemokines, and growth factors as an approach to further explore possible molecular mechanisms contributing to the Fn14-high tumor phenotype. Of note, one of these cytokines was the Fn14 ligand TWEAK, which was expressed at similar levels in normal brain, Fn14-low, and Fn14-high tumors. This result is consistent with prior TWEAK expression studies using human brain and GBM specimens (Hersh, Peng, et al., 2018; Tran et al., 2003) and implies that Fn14 overexpression itself (Brown et al., 2013; Tran et al., 2005), not increased TWEAK:Fn14 engagement, is likely driving the Fn14-high tumor phenotype. We identified several proteins that showed a large increase in expression in Fn14-high rat gliomas compared to normal brain or Fn14-low gliomas but here we focused on our top two hits: PDGF-B and PAI-1. Both of these multifunctional proteins are implicated in various aspects of tumor growth and metastasis (Cao, 2013; Kubala & DeClerck, 2019), but we found by querying human GBM datasets that PAI-1 was more likely to play a critical role in human Fn14-high GBM pathobiology. Specifically, the human PAI-1 (SERPINE1) gene was highly expressed in GBM compared to normal brain, and its expression level correlated with shorter survival, confirming prior work by other groups using smaller sample sizes (Colin et al., 2009; Roy et al., 2015; Seker et al., 2019; Vachher et al., 2020; Wang et al., 2020). Interestingly, analysis of Fn14 (Hersh, Harder, et al., 2018) and SERPINE1 (Wang et al., 2020) expression in patient-matched primary and recurrent GBM tumors has revealed that both genes are maximally expressed at recurrence. We also found that Fn14 and SERPINE1 were co-expressed at relatively high levels in the pseudopalisading cells surrounding necrotic regions and in microvascular proliferation zones. Elevated Fn14 expression in GBM regions containing pseudopalisading necrosis and vascularization is consistent with our IHC results ((Hersh, Harder, et al., 2018; Tran et al., 2003; Tran et al., 2006) and Figure 1(b)) while high SERPINE1 expression in these regions is consistent with a prior in situ hybridization study (Colin et al., 2009).

We also examined a GBM tumor scRNA-seq database to query potential cell types responsible for Fn14 and SERPINE1 gene expression within the TME and found that these two genes were expressed by malignant (i.e., tumor) cells and macrophages. There was a statistically significant positive correlation between the Fn14 and SERPINE1 gene expression level in tumor cells, suggesting Fn14 signaling in these cells could be driving PAI-1 expression in the rat Fn14-high gliomas. Since Fn14 overexpression alone can activate the NF-κB pathway (Brown et al., 2013; Tran et al., 2005) (Figure 5(a)) and SERPINE1 is

an NF-κB target gene (Friedmann-Morvinski et al., 2016), this is one potential mechanism for the observed correlation.

To our knowledge, there have been no prior reports demonstrating Fn14 or SERPINE1 gene expression in brain TAMs. Fn14 signaling is central to macrophage differentiation and function in numerous disease states (Burkly et al., 2011; Winkles, 2008). Given the finding that high Fn14 expression in the tumor cells more than TAMs appears to drive the aggressive GBM phenotype observed here, it is possible that Fn14 signaling coordinates some form of myeloid mimicry to enable tumor growth, brain invasion, and immune evasion (Bakhoum etal., 2018).

This study demonstrates that Fn14 regulates distinctive and pathognomonic features of gliomas, including specific MRI, histopathological, biochemical, and molecular characteristics, notably elevated NF-κB signaling and increased PAI-1 levels. Importantly, these effects occur without elevated levels of TWEAK, reinforcing the cell-autonomous signaling associated with high Fn14 expression. Although NF-κB activation in gliomas has been linked to mesenchymal differentiation (Bhat et al., 2013), and human mesenchymal-like GBMs exhibit many of the same properties as the rat Fn14-high tumors described here, including a high degree of necrosis (Cooper et al., 2012; Verhaak et al., 2010), increased TAM density (Kaffes et al., 2019; Verhaak et al., 2010), and upregulated SERPINE1 (Bhat et al., 2013; Roy et al., 2015; Seker et al., 2019), RELB (Verhaak et al., 2010; Zeng et al., 2019) and OPN (Wei et al., 2019) gene expression, additional RNA profiling experiments assaying the expression of proneural and mesenchymal subtype signature genes would be necessary to determine if Fn14 alone can trigger a full proneural-to-mesenchymal transition.

We postulate that PAI-1 activity in particular is contributing to the aggressive nature of the Fn14-high tumors given that PAI-1 depletion in glioma cells via shRNA transduction or siRNA treatment (i) inhibits glioma cell growth (Wang et al., 2020), migration (Seker et al., 2019) and invasion (Smith et al., 2020; Wang et al., 2020) in vitro, and (ii) reduces tumor growth in an orthotopic xenograft model in vivo (Seker et al., 2019). Also, PAI-1, as the primary physiological inhibitor of the serine proteases tPA and uPA and thus plasminogen-to-plasmin conversion, inhibits fibrinolysis (Urano et al., 2019). It has been proposed that GBM intravascular thrombosis (i.e., the formation of a fibrin-platelet clot and the classic intraoperative finding of “black veins”) may trigger hypoxia, necrosis, and glioma cell migration, leading to pseudopalisade formation (Rong et al., 2006). Thus, PAI-1 overexpression in the Fn14-high glioma TME likely contributes to the high degree of pseudopalisading necrosis and the increased lactate levels in the tumor core. It has also been reported that enhanced PAI-1 expression may contribute to an immune cell-rich TME (Saidak et al., 2020) and that tumor-derived PAI-1 increases macrophage infiltration into solid tumors (Kubala et al., 2018). Therefore, PAI-1, perhaps acting in concert with the macrophage chemokine OPN (Wei et al., 2019), which is also preferentially expressed in the rat Fn14-high tumors (Figure 5(b,c); Table 1), could contribute to the elevated TAM density observed in the Fn14-high tumors. Taken together, the results of this study elevate the importance of Fn14 in GBM pathobiology and identify both the NF-κB signaling node and PAI-1 as potential therapeutic targets for Fn14-high gliomas.

Supplementary Material

Refer to Web version on PubMed Central for supplementary material.

ACKNOWLEDGMENTS

This research was supported in part by National Institutes of Health (NIH) grants R01 NS107813 (G. F. W.), U01 CA220378 (N. L. T.), R01 CA187780 (E. E. B.), and R21 NS106553 (E. E. B.) and a University of Maryland Greenbaum Comprehensive Cancer Center Pilot Award (J. A. W.). N. P. C. was supported in part by NIH Training Grant T32 CA154274. The authors thank Pranjali Kanvinde for help with the Western blot quantitation and Sveta Ivanova (UMSOM Department of Neurosurgery) for help with the IF analyses.

DATA AVAILABILITY STATEMENT

The data that support the findings of this study are available from the corresponding author upon reasonable request.

REFERENCES

Bakhoum SF, Ngo B, Laughney AM, Cavallo JA, Murphy CJ, Ly P, … Cantley LC (2018). Chromosomal instability drives metastasis through a cytosolic DNA response. Nature, 553(7689), 467–472. 10.1038/nature25432 [PubMed: 29342134]

Bhat KPL, Balasubramaniyan V, Vaillant B, Ezhilarasan R, Hummelink K, Hollingsworth F, … Aldape K (2013). Mesenchymal differentiation mediated by NF-kappaB promotes radiation resistance in glioblastoma. Cancer Cell, 24(3), 331–346. 10.1016/j.ccr.2013.08.001 [PubMed: 23993863]

Bowman RL, Wang Q, Carro A, Verhaak RG, & Squatrito M (2017). GlioVis data portal for visualization and analysis of brain tumor expression datasets. Neuro-Oncology, 19(1), 139–141. 10.1093/neuonc/now247 [PubMed: 28031383]

Bren GD, Solan NJ, Miyoshi H, Pennington KN, Pobst LJ, & Paya CV (2001). Transcription of the RelB gene is regulated by NF-kappaB. Oncogene, 20(53), 7722–7733. 10.1038/sj.onc.1204868 [PubMed: 11753650]

Brown SA, Cheng E, Williams MS, & Winkles JA (2013). TWEAK-independent Fn14 self-association and NF-kappaB activation is mediated by the C-terminal region of the Fn14 cytoplasmic domain. PLoS One, 8(6), e65248. 10.1371/journal.pone.0065248 [PubMed: 23750247]

Burkly LC, Michaelson JS, & Zheng TS (2011). TWEAK/Fn14 pathway: An immunological switch for shaping tissue responses. Immunological Reviews, 244(1), 99–114. 10.1111/j.1600-065X.2011.01054.x [PubMed: 22017434]

Cahill KE, Morshed RA, & Yamini B (2016). Nuclear factor-kappaB in glioblastoma: Insights into regulators and targeted therapy. Neuro-Oncology, 18(3), 329–339. 10.1093/neuonc/nov265 [PubMed: 26534766]

Cancer Genome Atlas Research Network. (2008). Comprehensive genomic characterization defines human glioblastoma genes and core pathways. Nature, 455(7216), 1061–1068. 10.1038/nature07385 [PubMed: 18772890]

Cao Y (2013). Multifarious functions of PDGFs and PDGFRs in tumor growth and metastasis. Trends in Molecular Medicine, 19(8), 460–473. 10.1016/j.molmed.2013.05.002 [PubMed: 23773831]

Chaumeil MM, Lupo JM, & Ronen SM (2015). Magnetic resonance (MR) metabolic imaging in glioma. Brain Pathology, 25(6), 769–780. 10.1111/bpa.12310 [PubMed: 26526945]

Cheng E, Whitsett TG, Tran NL, & Winkles JA (2015). The TWEAK receptor Fn14 is an src-inducible protein and a positive regulator of src-driven cell invasion. Molecular Cancer Research, 13(3), 575–583. 10.1158/1541-7786.MCR-14-0411 [PubMed: 25392346]

Cherry EM, Lee DW, Jung JU, & Sitcheran R (2015). Tumor necrosis factor-like weak inducer of apoptosis (TWEAK) promotes glioma cell invasion through induction of NF-kappaB-inducing kinase (NIK) and noncanonical NF-kappaB signaling. Molecular Cancer, 14, 9. 10.1186/s12943-014-0273-1 [PubMed: 25622756]

Cloughesy TF, Cavenee WK, & Mischel PS (2014). Glioblastoma: From molecular pathology to targeted treatment. Annual Review of Pathology, 9, 1–25. 10.1146/annurev-pathol-011110-130324

Colin C, Voutsinos-Porche B, Nanni I, Fina F, Metellus P, Intagliata D, … Figarella-Branger D (2009). High expression of cathepsin B and plasminogen activator inhibitor type-1 are strong predictors of survival in glioblastomas. Acta Neuropathologica, 118(6), 745–754. 10.1007/s00401-009-0592-2 [PubMed: 19774387]

Connolly NP, Shetty AC, Stokum JA, Hoeschele I, Siegel MB, Miller CR, … Woodworth GF (2018). Cross-species transcriptional analysis reveals conserved and host-specific neoplastic processes in mammalian glioma. Scientific Reports, 8(1), 1180. 10.1038/s41598-018-19451-6 [PubMed: 29352201]

Connolly NP, Stokum JA, Schneider CS, Ozawa T, Xu S, Galisteo R, … Woodworth GF (2017). Genetically engineered rat gliomas: PDGF-driven tumor initiation and progression in tv-a transgenic rats recreate key features of human brain cancer. PLoS One, 12(3), e0174557. 10.1371/journal.pone.0174557 [PubMed: 28358926]

Cooper LA, Gutman DA, Chisolm C, Appin C, Kong J, Rong Y, … Brat DJ (2012). The tumor microenvironment strongly impacts master transcriptional regulators and gene expression class of glioblastoma. The American Journal of Pathology, 180(5), 2108–2119. 10.1016/j.ajpath.2012.01.040 [PubMed: 22440258]

Fortin SP, Ennis MJ, Savitch BA, Carpentieri D, McDonough WS, Winkles JA, … Tran NL (2009). Tumor necrosis factor-like weak inducer of apoptosis stimulation of glioma cell survival is dependent on Akt2 function. Molecular Cancer Research, 7(11), 1871–1881. 10.1158/1541-7786.MCR-09-0194 [PubMed: 19861406]

Fortin SP, Ennis MJ, Schumacher CA, Zylstra-Diegel CR, Williams BO, Ross JT, … Tran NL (2012). Cdc42 and the guanine nucleotide exchange factors Ect2 and trio mediate Fn14-induced migration and invasion of glioblastoma cells. Molecular Cancer Research, 10(7), 958–968. 10.1158/1541-7786.MCR-11-0616 [PubMed: 22571869]

Friedmann-Morvinski D, Narasimamurthy R, Xia Y, Myskiw C, Soda Y, & Verma IM (2016). Targeting NF-kappaB in glioblastoma: A therapeutic approach. Science Advances, 2(1), e1501292. 10.1126/sciadv.1501292 [PubMed: 26824076]

Gao W, Wang X, Li F, Shi W, Li H, & Zeng Q (2019). Cho/Cr ratio at MR spectroscopy as a biomarker for cellular proliferation activity and prognosis in glioma: Correlation with the expression of minichromosome maintenance protein 2. Acta Radiologica, 60(1), 106–112. 10.1177/0284185118770899 [PubMed: 29665708]

Gutmann DH, & Kettenmann H (2019). Microglia/brain macrophages as central drivers of brain tumor pathobiology. Neuron, 104(3), 442–449. 10.1016/j.neuron.2019.08.028 [PubMed: 31697921]

Hersh DS, Harder BG, Roos A, Peng S, Heath JE, Legesse T, … Winkles JA (2018). The TNF receptor family member Fn14 is highly expressed in recurrent glioblastoma and in GBM patient-derived xenografts with acquired temozolomide resistance. Neuro-Oncology, 20(10), 1321–1330. 10.1093/neuonc/noy063 [PubMed: 29897522]

Hersh DS, Peng S, Dancy JG, Galisteo R, Eschbacher JM, Castellani RJ, … Winkles JA (2018). Differential expression of the TWEAK receptor Fn14 in IDH1 wild-type and mutant gliomas. Journal of Neuro-Oncology, 138(2), 241–250. 10.1007/s11060-018-2799-3 [PubMed: 29453678]

Hersh DS, Wadajkar AS, Roberts N, Perez JG, Connolly NP, Frenkel V, … Kim AJ (2016). Evolving drug delivery strategies to overcome the blood brain barrier. Current Pharmaceutical Design, 22(9), 1177–1193. 10.2174/1381612822666151221150733 [PubMed: 26685681]

Kaffes I, Szulzewsky F, Chen Z, Herting CJ, Gabanic B, Velazquez Vega JE, … Hambardzumyan D (2019). Human mesenchymal glioblastomas are characterized by an increased immune cell presence compared to proneural and classical tumors. Oncoimmunology, 8(11), e1655360. 10.1080/2162402X.2019.1655360 [PubMed: 31646100]

Kampa JM, Kellner U, Marsching C, Ramallo Guevara C, Knappe UJ, Sahin M, … Bednarz H (2020). Glioblastoma multiforme: Metabolic differences to peritumoral tissue and IDH-mutated gliomas revealed by mass spectrometry imaging. Neuropathology, 40, 546–558. 10.1111/neup.12671 [PubMed: 32662157]

Kanvinde PP, Malla AP, Connolly NP, Szulzewsky F, Anastasiadis P, Ames HM, … Woodworth GF (2021). Leveraging the replication-competent avian-like sarcoma virus/tumor virus receptor—A system for modeling human gliomas. Glia, 10.1002/glia.23984. Online ahead of print.

Khalafallah AM, Huq S, Jimenez AE, Serra R, Bettegowda C, & Mukherjee D (2020). "Zooming in" on glioblastoma: Understanding tumor heterogeneity and its clinical implications in the era of single-cell ribonucleic acid sequencing. Neurosurgery, 88, 477–486. 10.1093/neuros/nyaa305

Kubala MH, & DeClerck YA (2019). The plasminogen activator inhibitor-1 paradox in cancer: A mechanistic understanding. Cancer Metastasis Reviews, 38(3), 483–492. 10.1007/s10555-019-09806-4 [PubMed: 31734763]

Kubala MH, Punj V, Placencio-Hickok VR, Fang H, Fernandez GE, Sposto R, & DeClerck YA (2018). Plasminogen activator inhibitor-1 promotes the recruitment and polarization of macrophages in cancer. Cell Reports, 25(8), 2177–2191 e2177. 10.1016/j.celrep.2018.10.082 [PubMed: 30463014]

Lee DW, Ramakrishnan D, Valenta J, Parney IF, Bayless KJ, & Sitcheran R (2013). The NF-kappaB RelB protein is an oncogenic driver of mesenchymal glioma. PLoS One, 8(2), e57489. 10.1371/journal.pone.0057489 [PubMed: 23451236]

Legarda-Addison D, & Ting AT (2007). Negative regulation of TCR signaling by NF-kappaB2/p100. Journal of Immunology, 178(12), 7767–7778. 10.4049/jimmunol.178.12.7767

Neftel C, Laffy J, Filbin MG, Hara T, Shore ME, Rahme GJ, … Suva ML (2019). An integrative model of cellular states, plasticity, and genetics for glioblastoma. Cell, 178(4), 835–849 e821. 10.1016/j.cell.2019.06.024 [PubMed: 31327527]

Ohtsu N, Nakatani Y, Yamashita D, Ohue S, Ohnishi T, & Kondo T (2016). Eva1 maintains the stem-like character of glioblastoma-initiating cells by activating the noncanonical NF-kappaB signaling pathway. Cancer Research, 76(1), 171–181. 10.1158/0008-5472.CAN-15-0884 [PubMed: 26677976]

Ostrom QT, Patil N, Cioffi G, Waite K, Kruchko C, & Barnholtz-Sloan JS (2020). CBTRUS statistical report: Primary brain and other central nervous system tumors diagnosed in the United States in 2013-2017. Neuro-Oncology, 22(12 Suppl 2), iv1–iv96. 10.1093/neuonc/noaa200 [PubMed: 33123732]

Ozawa T, Riester M, Cheng YK, Huse JT, Squatrito M, Helmy K, … Holland EC (2014). Most human non-GCIMP glioblastoma subtypes evolve from a common proneural-like precursor glioma. Cancer Cell, 26(2), 288–300. 10.1016/j.ccr.2014.06.005 [PubMed: 25117714]

Perez JG, Tran NL, Rosenblum MG, Schneider CS, Connolly NP, Kim AJ, … Winkles JA (2016). The TWEAK receptor Fn14 is a potential cell surface portal for targeted delivery of glioblastoma therapeutics. Oncogene, 35(17), 2145–2155. 10.1038/onc.2015.310 [PubMed: 26300004]

Provencher SW (2001). Automatic quantitation of localized in vivo 1H spectra with LCModel. NMR in Biomedicine, 14(4), 260–264. 10.1002/nbm.698 [PubMed: 11410943]

Puchalski RB, Shah N, Miller J, Dalley R, Nomura SR, Yoon JG, … Foltz GD (2018). An anatomic transcriptional atlas of human glioblastoma. Science, 360(6389), 660–663. 10.1126/science.aaf2666 [PubMed: 29748285]

Quail DF, & Joyce JA (2017). The microenvironmental landscape of brain tumors. Cancer Cell, 31(3), 326–341. 10.1016/j.ccell.2017.02.009 [PubMed: 28292436]

Rong Y, Durden DL, van Meir EG, & Brat DJ (2006). 'Pseudopalisading' necrosis in glioblastoma: A familiar morphologic feature that links vascular pathology, hypoxia, and angiogenesis. Journal of Neuropathology and Experimental Neurology, 65(6), 529–539. 10.1097/00005072-200606000-00001 [PubMed: 16783163]

Roos A, Dhruv HD, Mathews IT, Inge LJ, Tuncali S, Hartman LK, … Tran NL (2017). Identification of aurintricarboxylic acid as a selective inhibitor of the TWEAK-Fn14 signaling pathway in glioblastoma cells. Oncotarget, 8(7), 12234–12246. 10.18632/oncotarget.14685 [PubMed: 28103571]

Roos A, Dhruv HD, Peng S, Inge LJ, Tuncali S, Pineda M, … Tran NL (2018). EGFRvIII-Stat5 signaling enhances glioblastoma cell migration and survival. Molecular Cancer Research, 16(7), 1185–1195. 10.1158/1541-7786.MCR-18-0125 [PubMed: 29724813]

Roy A, Coum A, Marinescu VD, Polajeva J, Smits A, Nelander S, … Tchougounova E (2015). Glioma-derived plasminogen activator inhibitor-1 (PAI-1) regulates the recruitment of

LRP1 positive mast cells. Oncotarget, 6(27), 23647–23661. 10.18632/oncotarget.4640 [PubMed: 26164207]

Saidak Z, Soudet S, Lottin M, Salle V, Sevestre MA, Clatot F, & Galmiche A (2020). A pan-cancer analysis of the human tumor coagulome and its link to the tumor immune microenvironment. Cancer Immunology, Immunotherapy, 70, 923–933. 10.1007/s00262-020-02739-w [PubMed: 33057845]

Schindelin J, Arganda-Carreras I, Frise E, Kaynig V, Longair M, Pietzsch T, … Cardona A (2012). Fiji: An open-source platform for biological-image analysis. Nature Methods, 9(7), 676–682. 10.1038/nmeth.2019 [PubMed: 22743772]

Seker F, Cingoz A, Sur-Erdem I, Erguder N, Erkent A, Uyulur F, … Bagci-Onder T (2019). Identification of SERPINE1 as a regulator of glioblastoma cell dispersal with transcriptome profiling. Cancers (Basel), 11(11), 1651. 10.3390/cancers11111651

Smith SJ, Rowlinson J, Estevez-Cebrero M, Onion D, Ritchie A, Clarke P, … Rahman R (2020). Metabolism-based isolation of invasive glioblastoma cells with specific gene signatures and tumorigenic potential. Neuro-Oncology Advances, 2(1), 1. 10.1093/noajnl/vdaa087 [PubMed: 32642726]

Stupp R, Taillibert S, Kanner A, Read W, Steinberg D, Lhermitte B, … Ram Z (2017). Effect of tumor-treating fields plus maintenance temozolomide vs maintenance temozolomide alone on survival in patients with glioblastoma: A randomized clinical trial. Jama, 318(23), 2306–2316. 10.1001/jama.2017.18718 [PubMed: 29260225]

Sun SC, Ganchi PA, Ballard DW, & Greene WC (1993). NF-kappa B controls expression of inhibitor I kappa B alpha: Evidence for an inducible autoregulatory pathway. Science, 259(5103), 1912–1915. 10.1126/science.8096091 [PubMed: 8096091]

Tegowski M, & Baldwin A (2018). Noncanonical NF-kappaB in cancer. Biomedicines 6(2), 66. 10.3390/biomedicines6020066

Tran NL, McDonough WS, Donohue PJ, Winkles JA, Berens TJ, Ross KR, … Berens ME (2003). The human Fn14 receptor gene is up-regulated in migrating glioma cells in vitro and overexpressed in advanced glial tumors. The American Journal of Pathology, 162(4), 1313–1321. 10.1016/S0002-9440(10)63927-2 [PubMed: 12651623]

Tran NL, McDonough WS, Savitch BA, Fortin SP, Winkles JA, Symons M, … Berens ME (2006). Increased fibroblast growth factor-inducible 14 expression levels promote glioma cell invasion via Rac1 and nuclear factor-kappaB and correlate with poor patient outcome. Cancer Research, 66(19), 9535–9542. 10.1158/0008-5472.CAN-06-0418 [PubMed: 17018610]

Tran NL, McDonough WS, Savitch BA, Sawyer TF, Winkles JA, & Berens ME (2005). The tumor necrosis factor-like weak inducer of apoptosis (TWEAK)-fibroblast growth factor-inducible 14 (Fn14) signaling system regulates glioma cell survival via NFkappaB pathway activation and BCL-XL/BCL-W expression. The Journal of Biological Chemistry, 280(5), 3483–3492. 10.1074/jbc.M409906200 [PubMed: 15611130]

Urano T, Suzuki Y, Iwaki T, Sano H, Honkura N, & Castellino FJ (2019). Recognition of plasminogen activator inhibitor type 1 as the primary regulator of fibrinolysis. Current Drug Targets, 20(16), 1695–1701. 10.2174/1389450120666190715102510 [PubMed: 31309890]

Vachher M, Arora K, Burman A, & Kumar B (2020). NAMPT, GRN, and SERPINE1 signature as predictor of disease progression and survival in gliomas. Journal of Cellular Biochemistry, 121(4), 3010–3023. 10.1002/jcb.29560 [PubMed: 31710121]

Verhaak RG, Hoadley KA, Purdom E, Wang V, Qi Y, Wilkerson MD, … Cancer Genome Atlas Research Network. (2010). Integrated genomic analysis identifies clinically relevant subtypes of glioblastoma characterized by abnormalities in PDGFRA, IDH1, EGFR, and NF1. Cancer Cell, 17(1), 98–110. 10.1016/j.ccr.2009.12.020 [PubMed: 20129251]

Wang X, Bustos MA, Zhang X, Ramos RI, Tan C, Iida Y, … Hoon DSB (2020). Downregulation of the ubiquitin-E3 ligase RNF123 promotes upregulation of the NF-kappaB1 target serpinE1 in aggressive glioblastoma tumors. Cancers (Basel), 12(5), 1081. 10.3390/cancers12051081

Waters MR, Gupta AS, Mockenhaupt K, Brown LN, Biswas DD, & Kordula T (2019). RelB acts as a molecular switch driving chronic inflammation in glioblastoma multiforme. Oncogene, 8(6), 37. 10.1038/s41389-019-0146-y

Wei J, Marisetty A, Schrand B, Gabrusiewicz K, Hashimoto Y, Ott M, … Heimberger AB (2019). Osteopontin mediates glioblastoma-associated macrophage infiltration and is a potential therapeutic target. The Journal of Clinical Investigation, 129(1), 137–149. 10.1172/JCI121266 [PubMed: 30307407]

Winkles JA (2008). The TWEAK-Fn14 cytokine-receptor axis: Discovery, biology and therapeutic targeting. Nature Reviews. Drug Discovery, 7(5), 411–425. 10.1038/nrd2488 [PubMed: 18404150]

Woodworth GF, Dunn GP, Nance EA, Hanes J, & Brem H (2014). Emerging insights into barriers to effective brain tumor therapeutics. Frontiers in Oncology, 4, 126. 10.3389/fonc.2014.00126 [PubMed: 25101239]

Yang L, Lin C, Wang L, Guo H, & Wang X (2012). Hypoxia and hypoxia-inducible factors in glioblastoma multiforme progression and therapeutic implications. Experimental Cell Research, 318(19), 2417–2426. 10.1016/j.yexcr.2012.07.017 [PubMed: 22906859]

Zeng F, Wang K, Huang R, Liu Y, Zhang Y, & Hu H (2019). RELB: A novel prognostic marker for glioblastoma as identified by population-based analysis. Oncology Letters, 18(1), 386–394. 10.3892/ol.2019.10296 [PubMed: 31289510]

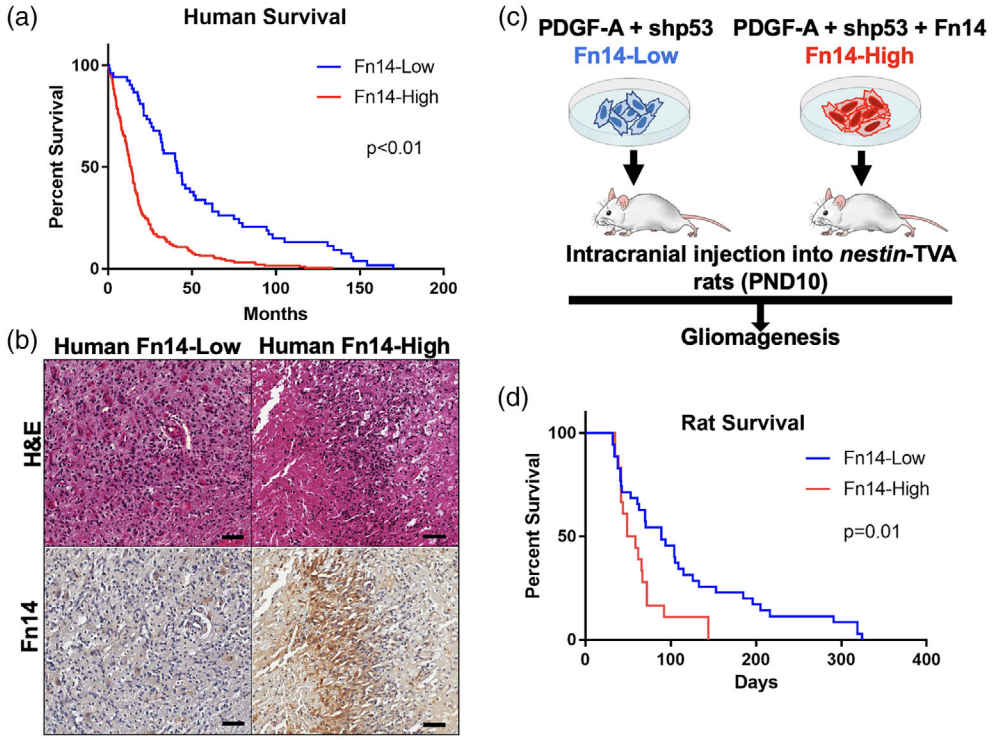

FIGURE 1.

High Fn14 gene expression in human glioblastoma (GBM) patient tumors and transgenic rat brain tumors correlates with shorter animal survival. (a) Kaplan–Meier survival analysis indicates that GBM patients with Fn14-high tumors have significantly lower survival rates compared to patients with Fn14-low tumors (Fn14-low median survival: 41.1 months, Fn14-high median survival: 13.7 months, $p < .01$). (b) H&E staining and Fn14 IHC analysis of representative human Fn14-low and Fn14-high tumor samples. Scale bar = 300 μm. (c) *Nestin* TV-A transgenic postnatal day (PND) 10 rats were injected with a combination of either PDGF-A + shp53 (Fn14-low) or PDGF-A + shp53 + Fn14 (Fn14-high) plasmid-transfected DF-1 cells. Animals were observed over time for tumor initiation and growth. (d) Kaplan–Meier survival analysis indicates that rats with Fn14-high tumors had significantly shorter survival times compared to rats with Fn14-low tumors (54 vs. 89 days, respectively; $p = .01$)

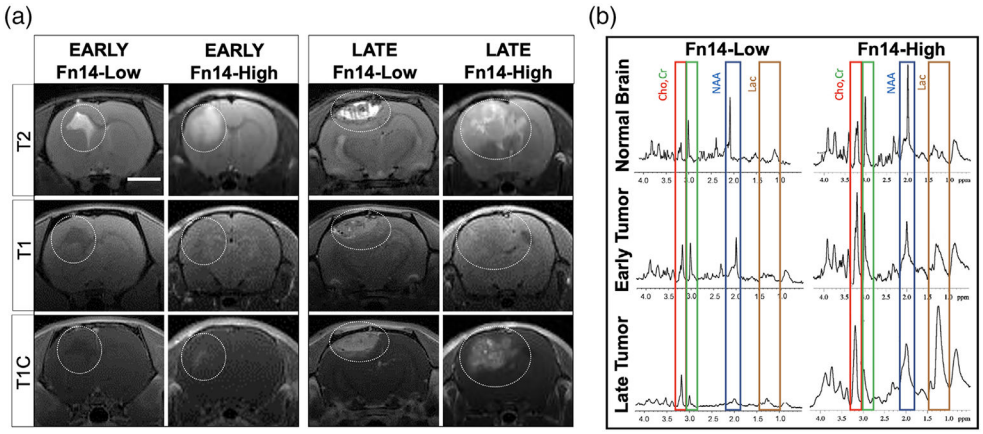

FIGURE 2.

Magnetic resonance imaging (MRI) and MR proton spectroscopy (MRS) reveals that Fn14-high tumors exhibit infiltrative patterns, marked contrast enhancement, and evidence of anaerobic metabolism, necrosis, and brain invasion. (a) Animals were scanned in the Bruker BioSpec horizontal bore MR scanner on three settings: T_2-weighted (T2), T_1-weighted without contrast (T1), and T_1-weighted with contrast (T1C) at early and late timepoints. Scale bar = 10 mm. (b) MRS was conducted on contralateral cerebral hemisphere (early timepoint animals; denoted here as normal brain) and on Fn14-low and Fn14-high brain tumors at both early and late timepoints. Values on the x-axis are chemical shift parts per million (PPM). Cho:Cr, choline:creatine (red and green box); Lac, lactate (brown box); NAA, *N*-acetylaspartate (blue box)

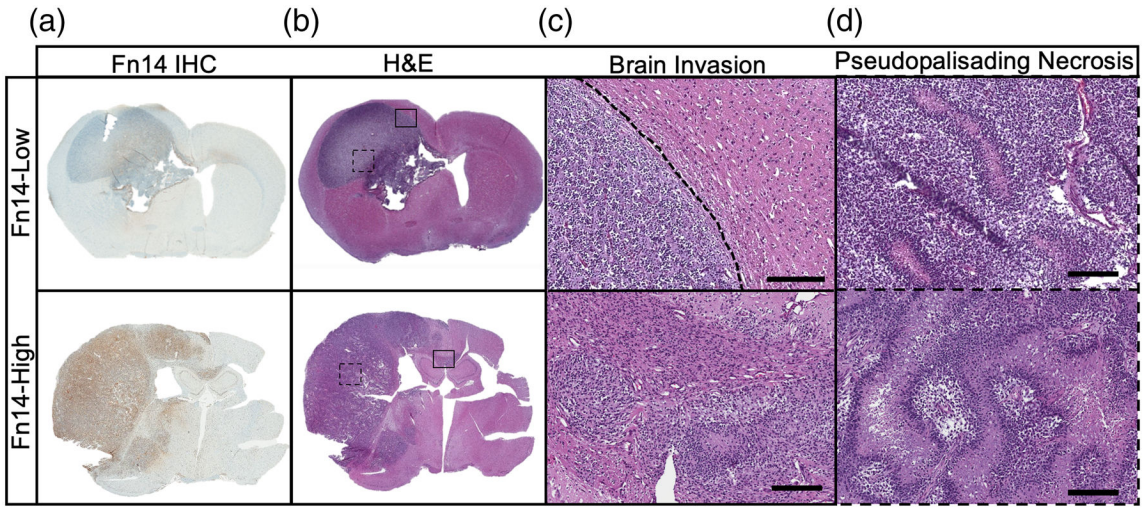

FIGURE 3.

Fn14-low and Fn14-high brain tumors have distinct histopathological features. Tissue sections prepared from representative Fn14-low and Fn14-high tumors were sectioned and processed for (a) Fn14 IHC analysis and (b) H&E staining. Two features commonly associated with high-grade human gliomas—brain invasion and pseudopalisading necrosis—are shown in the H&E panel as solid and dotted black boxes, respectively. (c) Higher magnification images of the invasion area solid box are shown, with a stippled line in the Fn14-low image demarcating the tumor and normal brain tissue boundary. (d) Higher magnification images of the tumor core region dotted black box with pseudopalisading necrosis are shown. Scale bar for (c) and (d) = 500 μm

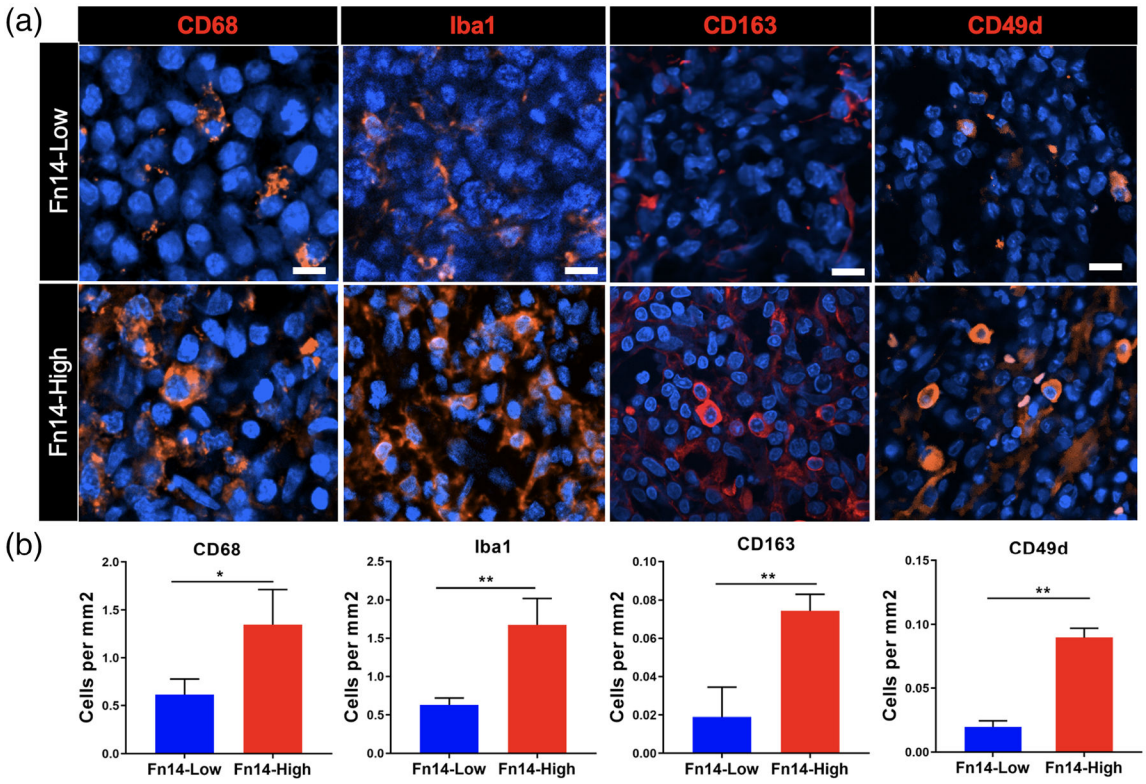

FIGURE 4.

The Fn14-high rat tumors have increased microglia/macrophage density when compared to the Fn14-low tumors. (a) Tissue sections prepared from representative Fn14-low and Fn14-high tumors were sectioned and processed for immunofluorescence analysis. Sections were incubated with primary antibodies detecting CD68 (activated M1-like macrophages), Iba1 (microglia/macrophages), CD163 (M2-like macrophages), and CD49d (bone marrow-derived macrophages). Scale bar = 50 μm. (b) Cell counts normalized to image area were analyzed for each macrophage marker. Macrophage density was significantly higher in Fn14-high tumors compared to Fn14-low tumors for all four markers. CD68 ($t(4) = 3.17$, $^{*}p < .05$), Iba1 ($t(4) = 5.103$, $^{**}p < .01$), CD163 ($t(4) = 5.411$, $^{**}p < .01$), CD49d ($t(4) = 13.87$, $^{**}p < .01$) (two-tailed Student's *t* test)

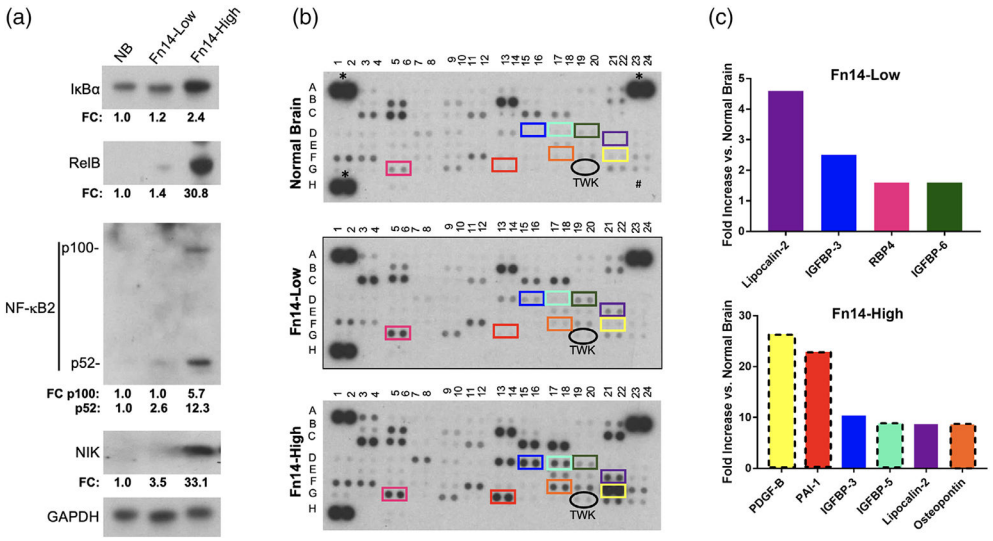

FIGURE 5.

Elevated Fn14 expression in rat proneural-like brain tumors promotes NF-κB signaling and alters the protein expression profile. (a) Normal brain (NB, cerebral cortex), Fn14-low, and Fn14-high tumors were lysed and Western blot analysis was conducted to detect the indicated proteins. Densitometry was used to quantitate the results, and the indicated protein levels were normalized to GAPDH levels and presented as fold expression relative to normal brain. (Fold change [FC]). (b) Normal brain, Fn14-low, and Fn14-high tumors were lysed and equivalent amounts of protein were incubated with nitrocellulose membranes containing antibodies directed to 79 rat cytokines, chemokines, and growth factors. Protein: antibody binding was assessed using streptavidin-HRP and chemiluminescence detection reagents. The spots (two per antibody) corresponding to the major proteins found to be upregulated in Fn14-low and/or Fn14-high tumors compared to normal brain are shown in colored boxes. In the normal brain panel, the three asterisks denote the positions of reference spots, and the hashtag denotes the position of negative control spots. The position on the array of the Fn14 ligand TWEAK (TWK) is circled on all three membranes. (c) The X-ray films were scanned and signal intensity of individual spots was quantitated using image analysis software. The four proteins showing a >1.5-fold increase in expression in the Fn14-low tumors compared to normal brain were lipocalin-2 (4.6-fold increase), IGFBP-3 (2.5-fold), RBP4 (1.6-fold), and IGFBP-6 (1.6-fold) (the bar colors correspond with the colored boxes in Panel (b)). The six proteins showing a >8.0-fold increase in the Fn14-high tumors compared to normal brain were PDGF-B (26.4-fold increase), PAI-1 (22.9-fold), IGFBP-3 (10.4-fold), IGFBP-5 (8.8-fold), lipocalin-2 (8.7-fold), and osteopontin (8.6-fold). Proteins uniquely upregulated in the Fn14-high tumors compared to normal brain and the Fn14-low tumors are shown with bars outlined by a stippled line. The bar colors correspond with the colored boxes in Panel (b)

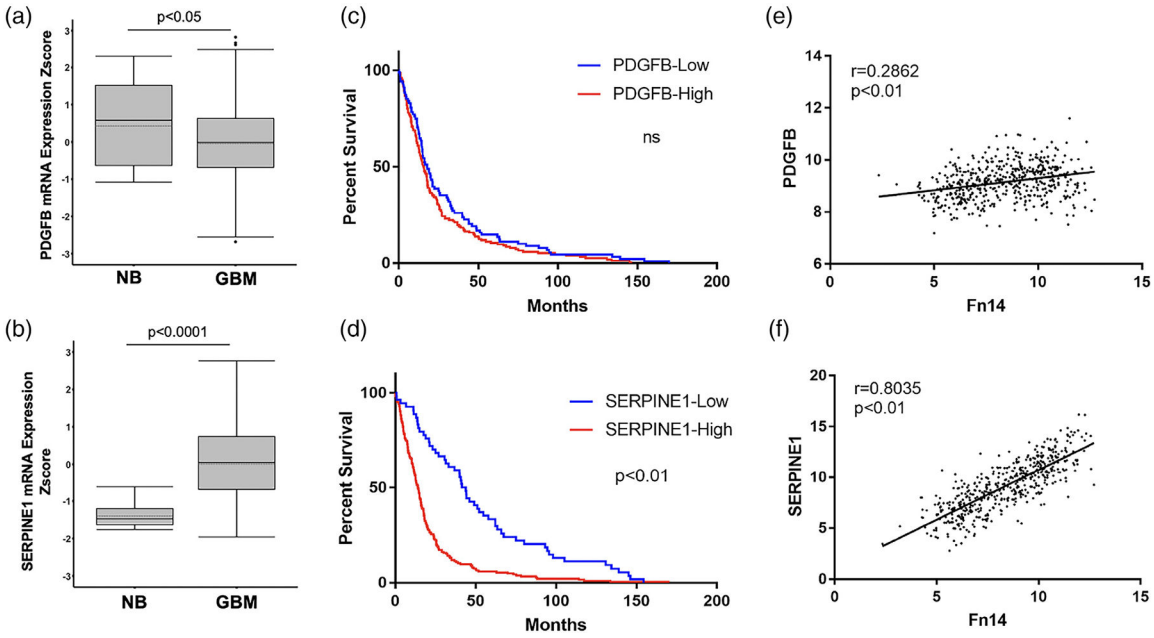

FIGURE 6.

The human PAI-1 (SERPINE1) gene is highly expressed in glioblastoma (GBM), which correlates with shorter patient survival and high Fn14 expression levels. (a) PDGFB and (b) SERPINE1 mRNA expression data in 10 nonneoplastic, normal brain (NB) and 548 GBM specimens were downloaded from the TCGA data portal and converted to *z*-scores. Patients used in this analysis were limited to the provisional TCGA dataset with gene expression availability for those two genes. Patient/sample sets for each expression cluster were plotted as box and whisker plots for each gene. The whiskers of the plot map the maximum and minimum *z*-score for each expression cluster. The bar and dotted bar in each box represent the median and mean value, respectively, for the expression *z*-score of each group. The top and bottom of each box represents the 25th and 75th percentile, respectively, of the expression *z*-score values for each group. PDGFB expression was significantly higher in NB specimens ($p < .05$) while SERPINE1 expression was significantly higher in GBM as compared to NB ($p < .0001$) as determined using Student's *t* test (two-tailed). Kaplan–Meier survival analysis indicates that (c) there is no correlation between PDGFB expression levels in human glioma patients and median survival time (PDGFB-low: 17.8-month median survival, PDGFB-high: 15.8-month median survival; $p = .1785$; ns = not significant) while (d) patients with SERPINE1-high tumors have significantly shorter survival rates compared to patients with SERPINE1-low tumors (SERPINE1-low: 43.9-month median survival, SERPINE1-high: 14.2-month median survival; $p < .01$). (e) PDGFB:Fn14 and (f) SERPINE1:Fn14 gene expression correlation analyses revealed that SERPINE1 and Fn14 were more frequently co-expressed at similar levels in gliomas (PDGFB:Fn14, $r = .2862$; SERPINE1:Fn14, $r = .8035$)

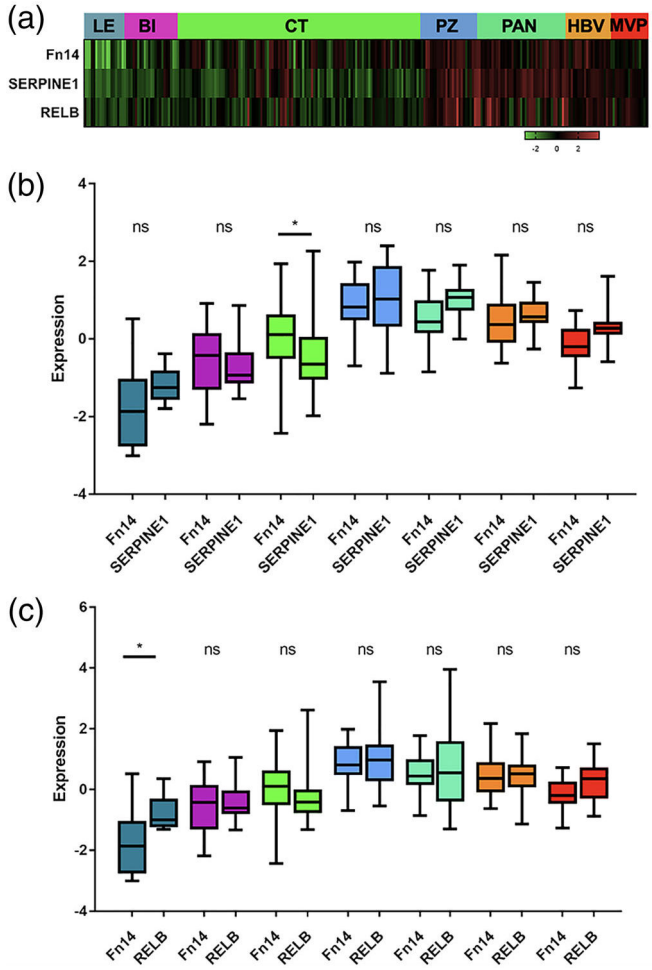

FIGURE 7.

Fn14, SERPINE1, and RELB are expressed at high levels in the same regions of GBM tumors. (a), A heat map delineating the Fn14, SERPINE1, and RELB mRNA expression range in tumor anatomic structures is shown. BI, brain invasion; CT, cellular tumor; HBV, hyperplastic blood vessels; LE, leading edge; MVP, microvascular proliferation; PAN, pseudopalisading cells around necrosis; PZ, perinecrotic zone. (b,c) The tumor region expression data shown in Panel (a) was quantitated and plotted with the bar colors corresponding to the colors shown at the top of Panel (a). Fn14 and SERPINE1 have a similar expression level in each tumor location (ns = not significant) except in the CT region where the expression level was significantly different (one-way ANOVA: $F(13,526) = 34.81$, $p < .01$; cellular tumor Fn14 ($M = -0.0146$, SD = 0.8474); cellular tumor SERPINE1 ($M = -0.4527$, SD = 0.8433), $p = .0011$). Fn14 and RELB have a similar expression level in each tumor location (ns = not significant) except in the LE region where the expression level was significantly different (one-way ANOVA: $F(13, 527) = 5.349$, $p < .01$; leading edge Fn14 (M = −1.8024, SD = 1.1238); leading edge RELB ($M = -0.8024$, SD = 0.5560), $p = .0108$)

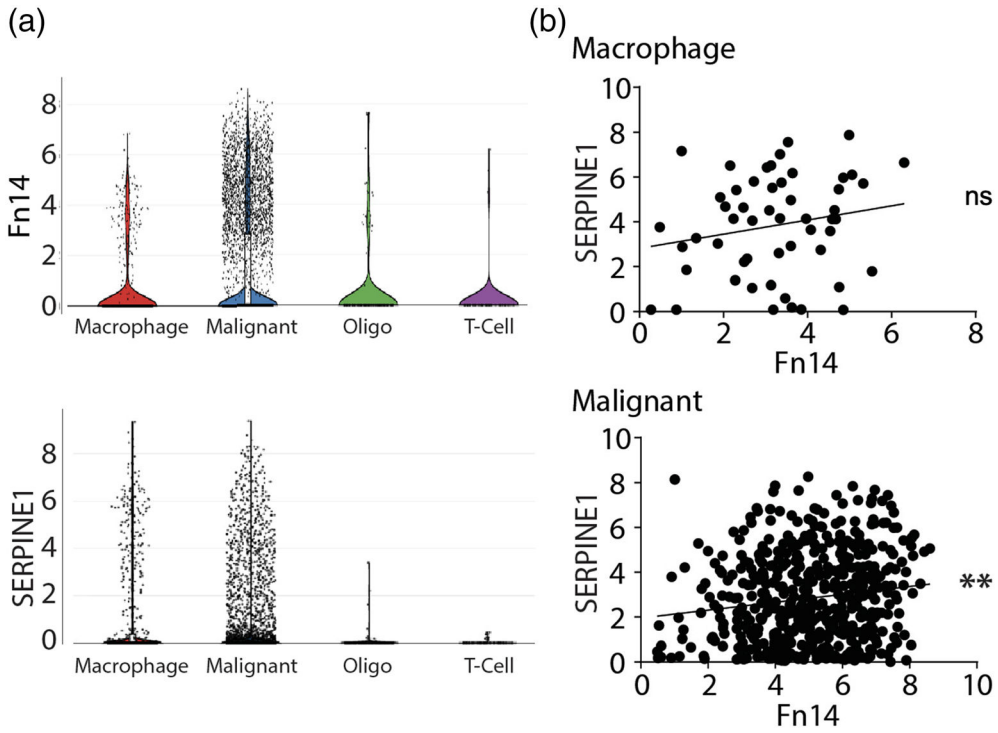

FIGURE 8.

The human Fn14 and SERPINE1 genes are expressed by both malignant cells and tumor-associated macrophages in the GBM tumor microenvironment. (a) Violin plots of single-cell RNA-seq data showing Fn14 and SERPINE1 are expressed in malignant cells and tumor-associated macrophages (TAMs) but rarely in oligodendrocytes or T-cells. (b) Pearson's correlation using single-cell RNA-seq data indicate that the expression of Fn14 and SERPINE1 is positively correlated in malignant cells ($r = .1434$, $^{**}p = .0012$) but not macrophages (ns = not significant)

TABLE 1

Protein profiling summary. The top 10 proteins upregulated in Fn14-low and Fn14-high rat tumors compared to normal rat brain as determined using R&D Systems Rat XL Cytokine Array Kit are listed. Proteins that are specifically overexpressed in the Fn14-high tumors compared to both normal brain and Fn14-low tumors are written in bold type

Normal brain vs. Fn14-low tumor		**Normal brain vs. Fn14-high tumor**	
Protein	**Fold-increase**	**Protein**	**Fold-increase**
Lipocalin-2	4.6	**PDGF-B**	26.4
IGFBP-3	2.5	**PAI-1**	22.9
RBP4	1.6	IGFBP-3	10.4
IGFBP-6	1.6	**IGFBP-5**	8.8
Galectin-3	1.3	Lipocalin-2	8.7
Adiponectin	0.8	**Osteopontin**	8.6
Fetuin-A	**0.7**	Adiponectin	4.9
IGFBP-2	0.6	IGFBP-2	4.0
RGM-A	0.5	Galectin-3	3.0
Osteoprotegerin	0.4	Osteoprotegerin	1.2